Direct numerical simulations of premixed and stratified flame propagation in turbulent channel flow

Andrea Gruber*
SINTEF Energy Research
7465, Trondheim, Norway

Edward S. Richardson
University of Southampton
SO17 1BJ Southampton, UK

Konduri Aditya and Jacqueline H. Chen
Sandia National Laboratories
Livermore, CA 94550, USA
(Dated: October 10, 2018)

Direct numerical simulations are performed to investigate the transient upstream flame propagation (flashback) through homogeneous and fuel-stratified hydrogen-air mixtures transported in fully-developed turbulent channel flows. Results indicate that, for both cases, the flame maintains steady propagation against the bulk flow direction and the global flame shape and the local flame characteristics are both affected by the occurrence of fuel stratification. Globally, the mean flame shape undergoes an abrupt change when the approaching reactants transition from an homogeneous to a stratified mixing configuration. A V-shaped flame surface, whose leading-edge is located in the near-wall region, characterizes the non-stratified, homogeneous mixture case while a U-shaped flame surface, whose leading-edge propagates upstream at the channel centreline, distinguishes the case with fuel stratification (fuel-lean in the near-wall region and fuel-rich away from the wall). The characteristic thickness, wrinkling and displacement speed of the turbulent flame brush are subject to considerable changes across the channel due to the dependence of the turbulence and mixture properties on the distance from the channel walls. More specifically, the flame transitions from a moderately wrinkled, thin-flamelet combustion regime in the homogeneous mixture case to a strongly wrinkled flame brush more representative of a thickened-flame combustion regime in the near-wall region of the fuel-stratified case. The combustion regime may be related to Karlovitz number and it is shown that a *nominal* channel-flow Karlovitz number, Ka_{in}^{ch}, based on the wall-normal variation of canonical turbulence ($t_\eta = (\nu/\epsilon)^{1/2}$) and chemistry ($t_l = \delta_l/S_l$) time scales in fully-developed channel flow, compares well with an *effective* Karlovitz number, Ka_{fl}^{ch}, extracted from the present DNS datasets using conditionally sampled values of t_η and t_l in the immediate vicinity of the flame ($0.1 < C < 0.3$).

I. INTRODUCTION

A. Background and Motivation

The process of unsteady flame propagation in turbulent, confined flows is of great importance for many industrial applications. State-of-the-art gas turbine combustors, scramjets and, generally, many recent internal combustion engines operate, more often than in the past, at increasingly high power densities that result in relatively large surface-to-volume ratios for the combustion chamber. The practical implementation of this trend is typically accompanied by the common occurrence of reactive flows where the flame is anchored or freely propagates in confined ducts, channels or vessels whose size is increasingly small relative to the size of the flame. If operated in a premixed fashion, such combustion systems are likely to be operated on the border of the stable flame region [1] and are often subject to thermo-acoustic instabilities, flame blow-out or flashback. Flashback is characterized by unsteady often abrupt and rapid flame propagation upstream of the flame's design position into the premixing section of the burner and understanding this process is the objective of the present study.

It is well-known that flashback is characterized by a number of different initiating mechanisms [2]. Flashback that occurs near the burner walls in the boundary layer of the flow is known as boundary layer flashback and is a safety issue for non-conventional and highly reactive fuels containing hydrogen. A recent comprehensive review [3] summarizes the status of knowledge on the physical mechanism behind boundary layer flashback in non-swirling flows, highlighting the challenges presented by the eventual adoption of fuels with increased reactivity. The addition of even small quantities of hydrogen to less reactive hydrocarbon fuels can alter the reactivity of these fuels in a drastic non-linear fashion [4, 5]. The reason for this is due to the specific combustion characteristics of hydrogen, recently summarized by Sanchez and Williams [6], that ultimately reduce the flame quench-

* andrea.gruber@sintef.no

ing distance [7] and therefore is able to support relatively high flame speed in the low-velocity region of the flow very close to the wall. Accordingly, the adoption of hydrogen-containing fuels introduces a number of design issues in state-of-the-art gas turbines [8] where the occurrence of the flame flashback process is often complicated further by the swirling pattern of the underlying turbulent flow. See Refs. [9, 10] for a recent excellent experimental characterization of flashback in swirling flows.

A practical design feature in gas turbine burners that considerably complicates the understanding of unsteady flame propagation during flashback is the presence of fuel-oxidant stratification and partial premixing. Here, the term *partially premixing* refers to compositionally-inhomogeneous mixtures that include flammable and non-flammable fluid, while *stratification* refers to a reacting front propagating through a mixture containing a range of compositions within the flammability limits [11]. Once flashback is initiated and the flame propagates upstream into the mixing section of the burner, the flame encounters a progressively less homogeneous flow of reactants, either temporarily, as a consequence of a transient perturbation of the fuel system flow rate, or permanently, as the flame establishes itself within the premixer section of the burner. In fact, it is reasonable to assume that, during a typical flashback event, flame propagation begins in conditions of *premixed combustion* at the flame design position, first evolving towards a *stratified combustion* situation, followed by propagation in *partially premixed* conditions that eventually leads to extinction or, if the flame survives, to *non-premixed combustion* if the flame anchors directly at the injection nozzles according to the flame-flow interaction mechanism [12–15]. It is also important to mention that, in modern low-emissions industrial burners, some degree of unmixedness, occurring either as partially-premixed reactants or as fuel-oxidant stratification, is often an intentional design feature, even at the flame design position, in order to achieve good flame stability properties [16]. For these reasons, the present work aims to achieve accurate insight and good understanding of flame propagation behaviour in confined flows of reactants that are characterized by a spatial variation of the reactant composition within the flammability limits (stratification).

B. Previous Work on Boundary Layer Flashback

The seminal paper by Lewis and von Elbe [17] is the first study to systematically investigate flashback limits and has remained as the state-of-the-art for order-of-magnitude flashback prediction. However this pioneering model from 1943, in determining the critical velocity gradient for the onset of flashback, erroneously assumes that the premixed flame propagating along the wall boundary layer has no effect on the approaching flow of reactants. In the past, practical difficulties in performing accurate experimental measurements in the near-wall region of reactive flows have represented a considerable challenge and only recently improved laser-based diagnostic techniques have enabled the acquisition of high-quality empirical data on flame-wall interactions [18] and near-wall flame propagation [19]. Recent experimental and numerical investigations of swirling and non-swirling reactive flows [10, 19–21] have revealed the presence of flame-induced flow reversals in the viscous layer ($y^+ \lesssim 20$) immediately upstream of the flame surface. These flow reversal "pockets" are consistently associated with regions of the flame front that are convex towards the reactants. In non-swirling flows, the convex leading-edge "bulges" of the flame front are, in turn, clearly correlated with the low-velocity streaks of the turbulent boundary layer [21]. These recent findings provide a radically different picture of the mechanism of boundary layer flashback and also underscores the need for near-wall flame propagation models that correctly accounts for this new conceptual understanding[22–24].

Early studies on flashback, building on the methodology proposed in Ref. [17], tried to chart the flashback behaviour of premixed flames in the transition from laminar flow to the more interesting case of turbulent flow and empirical observations showed a considerable increase of the critical velocity gradient in the presence of turbulence [25, 26]. This increase is consistent with the interpretation of the flashback mechanism for turbulent flames provided in [21] that highlights the limitations of a flashback theory ultimately based on a velocity balance within the quasi-laminar viscous layer. More recent modelling studies [27–29] have taken into account local Lewis number and flame curvature effects on the onset of laminar boundary layer flashback. However these analyses often consider flame surface curvature and displacement speed effects only by taking into account the wall-normal direction, and therefore are restricted by the assumption that boundary layer flashback is governed by physical processes whose main characteristics are two-dimensional.

The recent direct numerical simulations (DNS) performed by the present research group suggest that three-dimensional effects play a fundamental role in turbulent flame-wall interactions in general [30] and in the physical mechanism behind boundary layer flashback in particular [21, 22]. The presence in the fresh reactants of relatively low-velocity fluid organized in thin, elongated streaky regions, very close to the wall, provides ideal "trails" along which flame tongues at the front's leading-edge can advance, "slipping" underneath the bulk flow, to achieve upstream propagation during flashback. The three-dimensional nature of this process has a central role: even if the velocity gradient at the wall associated with the turbulent boundary layer is, in the mean, above the critical value for flashback to occur, the flame front can still encounter, locally, wall velocity gradients well below the critical value within the low-velocity streaky regions, ultimately resulting in leading point flame propagation.

The conceptual picture drawn above highlights the key

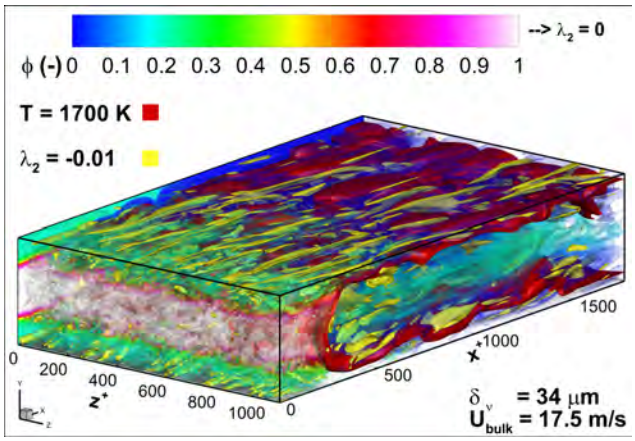

FIG. 1. Upstream flame propagation during flashback in a stratified mixture: the red surface demarcates a fluid temperature of $T = 1700\,[K]$ while the channel flow turbulence is visualized using the second eigenvalue of the vorticity gradient tensor, λ_2. The non-translucent yellow isosurfaces correspond to relatively strong vorticity within the near-wall coherent structures of the boundary layer, $\lambda_2 = -0.01$, while the local equivalence ratio is represented using the colour scale shown using transparency on the $\lambda_2 = 0.0$ isosurfaces.

role that spatial and temporal variations in fluid momentum play in near-wall flame propagation, but it does not consider the effect of variations in the fluid's composition and reactivity. These too are expected to affect the competition between fluid velocity and flame surface displacement speed, and to affect the flame propagation characteristics, both locally and globally.

Stratified combustion has been the subject of numerous modelling and experimental studies in recent years and the interested reader is advised to examine the careful review by Masri [11]. Most fundamental experimental studies of turbulent stratified combustion have considered unconfined flow configurations, for example free shear flows with different fuel/air blends introduced through concentric tubes. A few laboratory studies have examined stratification effects in small technical burners, as a model for combustion processes found in gas turbine combustors. However, none of these studies about stratified combustion have specifically considered confined flame propagation in ducts or channel configurations that would allow for a detailed investigation of flame-wall interactions and flashback.

The objective of the present study is to investigate unsteady propagation of a stratified flame during a flashback event that occurs in fully-developed turbulent channel flow. This configuration is similar to the one adopted in [21]; however, in the new case considered here, a compositional inhomogeneity is introduced at the channel inlet: specifically, fuel-lean conditions are imposed in the near-wall regions while the mixture is fuel-rich in the bulk flow around the channel centreline. After the initial transition from premixed to stratified combustion, the compositional stratification introduced here ultimately results in a turbulent flame steadily propagating upstream against the bulk flow direction with the leading-edge at the channel centreline, see Fig. 1. This new DNS database enables a detailed comparison versus the premixed cases already discussed in [21] and [22]. Accordingly, the present DNS builds upon and complements the earlier DNS and high-resolution experimental studies [19, 21, 22, 30–33] that were also conducted in the framework of the BIGCO2/BIGCCS/NCCS *R&D* platforms (http://www.nccs.no).

The remainder of this paper is organized as follows: the DNS code and the problem formulation are described in Section II. A comprehensive analysis of the DNS results from the new stratified mixture case along with a comparison with earlier results from the homogeneous mixture case are presented in Section III. Finally, conclusions and recommendations for further work are presented in Section IV.

II. MATHEMATICAL FORMULATION, CASE CONFIGURATION AND DNS CODE

The Navier-Stokes equations in their compressible formulation are solved in a three-dimensional computational domain to simulate the upstream propagation of non-anchored, premixed and stratified H_2-air flames in fully developed turbulent channel flow at a pressure of $2\,[atm]$ and at a global equivalence ratio varying between $\phi \sim 0.55$ (stationary value) and $\phi \sim 0.7$ (peak transient value). We shall refer to the three spatial directions in the computational domain as: streamwise direction (x), wall-normal direction (y) and spanwise direction (z). In the comparison reported below, the earlier premixed case and the present stratified case are denoted as $TCF055_h$ and $TCF055_s$, respectively, and these subscripts are used consistently in the remainder of the present paper.

Thermodynamic properties are modelled as polynomial functions of temperature and transport coefficients as described in the CHEMKIN and TRANSPORT packages, respectively [34]. Radiative heat transfer is not considered in this study and the temperature of the walls and of the reactants is set to $750\,[K]$ for both $TCF055_h$ and $TCF055_s$. The chemical reactions in the gas phase are described by a detailed mechanism for hydrogen combustion in air [35]. This mechanism consists of 9 species and 19 elementary reaction steps, see Table I for details. Nitrogen is assumed to be inert such that NO_x-formation reactions are not considered. The stratification of the reactant mixture entering the channel is introduced by imposing, at the domain inlet ($x = 0$), a spatial variation of the local equivalence ratio that is smoothly adjusted between a fuel-lean value of $\phi \sim 0.2$ in the near-wall region and a fuel-rich value of $\phi \sim 1.2$ in the bulk flow, see Fig. 2.

The Reynolds number of the approach flow is $Re_0 \sim 3200$ for both cases considered here, based on the chan-

TABLE I. The complete 9-species, 19-reactions hydrogen-air chemical kinetics mechanism from [35].

n	Reaction	B	a	E_a
1	$O_2 + H \Leftrightarrow OH + O$	3.547×10^{15}	-0.406	1.6599×10^4
2	$H_2 + O \Leftrightarrow OH + H$	0.508×10^5	2.67	0.629×10^4
3	$OH + H_2 \Leftrightarrow H + H_2O$	0.216×10^9	1.51	0.343×10^4
4	$H_2O + O \Leftrightarrow 2OH$	2.97×10^6	2.02	1.34×10^4
5	$H_2 + M \Leftrightarrow 2H + M$	4.577×10^{19}	-1.40	1.0438×10^5
6	$2O + M \Leftrightarrow O_2 + M$	6.165×10^{15}	-0.50	0.0
7	$H + O + M \Leftrightarrow OH + M$	4.714×10^{18}	-1.00	0.0
8	$OH + H + M \Leftrightarrow H_2O + M$	3.800×10^{22}	-2.00	0.0
9	$O_2 + H(+M) \Leftrightarrow HO_2(+M)$	1.475×10^{12}	0.60	0.0
10	$H + HO_2 \Leftrightarrow O_2 + H_2$	1.66×10^{13}	0.00	0.823×10^3
11	$H + HO_2 \Leftrightarrow 2OH$	7.079×10^{13}	0.00	2.95×10^2
12	$O + HO_2 \Leftrightarrow OH + O_2$	0.325×10^{14}	0.00	0.0
13	$OH + HO_2 \Leftrightarrow O_2 + H_2O$	2.890×10^{13}	0.00	-4.970×10^2
14	$2HO_2 \Leftrightarrow O_2 + H_2O_2$	4.200×10^{14}	0.00	1.1982×10^4
15	$H_2O_2(+M) \Leftrightarrow 2OH(+M)$	2.951×10^{14}	0.00	4.843×10^4
16	$H + H_2O_2 \Leftrightarrow OH + H_2O$	0.241×10^{14}	0.00	0.397×10^4
17	$H + H_2O_2 \Leftrightarrow H_2 + HO_2$	0.482×10^{14}	0.00	0.795×10^4
18	$O + H_2O_2 \Leftrightarrow HO_2 + OH$	9.550×10^6	2.00	3.970×10^3
19	$OH + H_2O_2 \Leftrightarrow H_2O + HO_2$	5.800×10^{14}	0.00	9.557×10^3

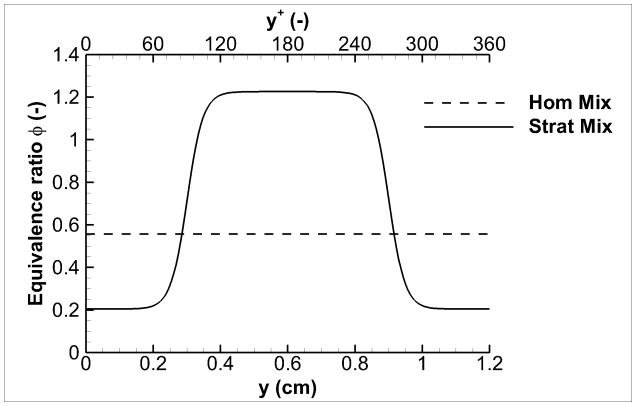

FIG. 2. Profile of equivalence ratio (ϕ) versus wall-distance in dimensional (y) and non-dimensional form (y^+) illustrating the imposed spatial variation in mixture composition at the domain inlet, $x = 0$.

nel mean centreline velocity U_c^f of the fresh reactants and the channel half-width h. This corresponds to a friction Reynolds number, $Re_\tau \sim h/\delta_\nu \sim 180$, where δ_ν is the viscous length scale. All turbulent quantities used below for non-dimensionalization characterize the turbulent flow of the fresh reactants upstream of the flame. The *wall Damköhler number* Da^w is the ratio of turbulent and chemical timescales that characterizes the combustion regime of turbulent flames in the near-wall regions of the flow. The conditions simulated give $Da_h^w \sim 0.69$ and $Da_s^w \sim 0.06$ for the premixed and stratified cases, respectively. As suggested in Ref. [30], these wall Damköhler numbers Da^w are based on the freely propagating one-dimensional laminar flame time scale ($t_{lh} = \delta_{lh}/S_{lh} \sim 4.8e^{-05}\,[s]$ and $t_{ls} = \delta_{ls}/S_{ls} \sim 5.3e^{-04}\,[s]$) and on the wall time scale that is uniquely defined from the turbulent channel flow of the fresh reactants ($t_{wh} = t_{ws} = \nu/u_\tau^2 \sim 3.3e^{-05}\,[s]$. In these expressions u_τ is the friction velocity, ν is the kinematic viscosity of the fresh reactants, and $\delta_{lh,s}$ and $S_{lh,s}$ are the laminar flame thickness and laminar flame velocities for the equivalence ratios present in the near-wall regions for the premixed and stratified case indicated by subscript h and s, respectively. It should be noted that the flame thickness, $\delta_{lh,s}$, at $\phi = 0.55$ and $\phi = 0.2$, respectively are estimated in terms of the fuel reaction rate thickness. Other relevant parameters of the DNS are given in Tab. II. Note that the non-dimensional mean centreline velocity is $u_c^+ \sim U_c^f/u_\tau \sim 19$ and channel bulk velocity is $U_{blk} = 17.5[m/s]$.

The turbulent H_2-air mixture, with a fuel mass flow rate of approximately $\sim 0.1[g/s]$ for both the premixed and the stratified case, enters the channel from a partially non-reflecting inflow boundary at $x = 0$ and approaches the flame in the streamwise direction while the burnt products leave the computational domain from a partially non-reflecting outflow boundary at $x = L_x$. Inflow and outflow boundary conditions are implemented following the Navier-Stokes Characteristic Boundary Conditions (NSCBC) methodology and are based on the original formulation of [36], incorporating the later improvements described in [37], [38] and [39] that include source and transverse terms. No-slip isothermal wall boundaries ($y = 0$ and $y = L_y$) are implemented following the methodology described in [40] and [33] for solid (non-porous) surfaces. Periodic (cyclic) boundary conditions are adopted in the spanwise direction ($z = 0$ and $z = L_z$) which results in statistical homogeneity in the z-direction, providing increased sample size for statistical analysis and averaging. The wall is assumed to be impermeable, so the wall-normal mass flux of all chemical species is set to zero.

The three-dimensional Cartesian grid is uniform in all directions. The first point from the wall is at $y^+ = 0.73$ where the superscript + indicates non-dimensionalization by the viscous length scale. There are 13 points within $y^+ = 10$ to satisfy the resolution requirements in the viscous layer [41]. The grid resolution is $\Delta x^+ = \Delta y^+ = \Delta z^+ = 0.73$ (equivalent to $25\,\mu m$) in both the premixed and the stratified case. The grid is not stretched, not even in the wall-normal direction, in order to accurately represent the flame which requires high spatial resolution throughout the channel, including near the centreline. See Tab. III for an overview of the DNS parameters.

A. Initialization and Transition from Premixed to Stratified Combustion

The reactive, premixed case is initialized using an auxiliary non-reacting flow solution, following the same procedure described in [21]. This is implemented by imposing at time, $t_h^0 = 0\,[s]$, a constant pressure value equal to $2\,[atm]$ throughout the domain, and instantaneous fluctuating velocity, density and temperature fields

TABLE II. Physical parameters for the simulated reactive cases: ϕ_w is the near-wall equivalence ratio, h the channel half-width, δ_ν the viscous length scale and Da^w the Damköhler number that describes the near-wall combustion regime.

Case Name	ϕ_w	U_c^f	h	$L_x \times L_y \times L_z$	δ_ν	S_l/U_c^f	Da^w	convective transit time (effective)
TCF055h	0.55	$20(m/s)$	$6(mm)$	$10h \times 2h \times 6h$	$3.4e^{-05}(m)$	0.35	0.69	1.5 [ms]
TCF055s	$0.20 - 1.20$	$20(m/s)$	$6(mm)$	$10h \times 2h \times 6h$	$3.4e^{-05}(m)$	$0.059 - 0.65$	$0.06 - 0.85$	1.5 [ms]

TABLE III. DNS parameters for the auxiliary non-reactive DNS and for the premixed and stratified reactive DNS: L is the domain length and N is the number of points used in the x, y and z directions respectively; h is the channel half-width; NRI: non-reflecting inlet; NRO: non-reflecting outlet; INSW: inert no-slip wall; PERIODIC: cyclic boundary condition.

Case Name	$L_x \times L_y \times L_z$	$N_x \times N_y \times N_z$	Δ^+	x_0/x_L	y_0/y_L	z_0/z_L
TCFAUX	$10h \times 2h \times 6h$	$760 \times 360 \times 560$	2.3/1.0/1.9	PERIODIC	INSW/INSW	PERIODIC
TCF055h	$10h \times 2h \times 6h$	$2400 \times 480 \times 1440$	0.73	NRI/NRO	INSW/INSW	PERIODIC
TCF055s	$10h \times 2h \times 6h$	$2400 \times 480 \times 1440$	0.73	NRI/NRO	INSW/INSW	PERIODIC

computed in the auxiliary non-reacting simulation. This procedure ensures that the flame encounters realistic approaching turbulence from the beginning of the simulation, thereby enabling a relatively short settling time. A one-dimensional premixed laminar flame placed in the middle of the domain is superimposed on the initial velocity field obtained from the auxiliary simulation. Burnt adiabatic product conditions are imposed downstream of the flame and an adjustment of the streamwise velocity field component is implemented for compatibility with the lower density on the product side of the flame. A progress variable function C is used in the initialization to map all points in the three-dimensional domain to one-dimensional CHEMKIN PREMIX [34] solutions for freely propagating planar H_2-air premixed flames. The progress variable C is a scalar parametrization of the reactive flow field, based on the water vapour mass fraction, that is equal to zero in the fresh reactants and unity in the burnt products.

The initialization technique described above yields a marginally incorrect initial pressure field. Therefore, an initial 'settling' time interval of at least five times the effective acoustic channel transit time ($10h/c \sim 8.2e^{-05}\,[s]$) is required for the initial pressure fluctuations to exit the domain from the inlet and outlet boundaries. After this initial settling time interval, $\Delta t_h^{tran} \sim 4.1e^{-04}\,[s]$, the turbulence-flame interaction is no longer affected by the initial pressure fluctuations and at this point the premixed flame has been wrinkled by the approaching turbulence and has begun to propagate upstream.

Following this initial "start-up" transient Δt_h^{tran}, statistically-steady upstream flame propagation occurs in the approaching turbulent channel flow of a lean ($\phi = 0.55$), homogeneous hydrogen-air mixture [22]. After approximately $1.1e^{-03}\,[s]$ of statistically-steady upstream flame propagation that has allowed for the acquisition of a satisfactory number of samples for analysis (see below), the inlet boundary condition for the mixture composition is transitioned (beginning at time $t_s^0 = 1.5e^{-03}\,[s]$) to the stratified mixture distribution with equivalence ratio variation across the channel width as shown in Fig. 2. The total mass flow of the hydrogen fuel entering the channel is slightly increased to emulate the occurrence of a transient surge in the fuel system mass flow that increases the global equivalence ratio of the mixture from $\phi = 0.55$ to $\phi \sim 0.7$ temporarily. While remaining overall fuel-lean, the stratified combustion case is designed to be locally fuel-rich at the channel centreline and fuel-lean at the walls. The newly introduced stratified reactants' mixture is convected downstream with the bulk flow and, as it reaches the turbulent flame brush, at time $t \sim 2.2e^{-03}$ approximately, it affects its reactivity, altering the local balance between the flame surface displacement speed and the underlying fluid velocity. A further transition period Δt_s^{tran} is observed in the solution as the flame adapts to the spatially varying mixture and ultimately results in a drastic change in the global flame shape. The transition from statistically-steady premixed to statistically-steady stratified flame propagation is completed at time $t \sim 3.0e^{-03}\,[s]$. Sampling of the statistically-steady stratified flame propagation process is initiated at $t \sim 3.0e^{-03}\,[s]$.

Due to the intrinsic transient characteristics of this particular flame configuration, results are sampled relatively frequently at every 1.21 wall time units, $t_w = 3.3e^{-05}\,[s]$. This is to ensure there is a sufficient number of samples in the database for future statistical post-processing. The sampling intervals for the premixed case and for the stratified case are reported in Tab. IV and result in a total of 27 and 25 samples, respectively. The numerical integration time step is fixed at a value, $\Delta t = 4.0e^{-09}\,[s]$ in the reactive case, and at $\Delta t = 1.0e^{-08}\,[s]$ in the inert auxiliary simulation, corresponding to 8250 and 3300 time steps per wall time unit, respectively.

The parallel DNS code, S3D [42], is used to perform the present DNS. In addition to the previous flame-wall interaction study [21, 22, 30, 33], S3D has been used for a range of studies, including a wide range of flame types: premixed flames [43–45], non-premixed flames [12–15, 46, 47], stratified [48, 49] and autoignition stabilized flames [50–52].

S3D is written in FORTRAN 90 and uses the Mes-

TABLE IV. Overview of settling time intervals and sampling time intervals for the premixed and stratified cases.

Case Name	Time Interval Name	Description	Actual Times
TCF055h	t_h^0	PMX DNS Starts	$t = 0\,[s]$
	Δt_h^{tran}	PMX Settling Time	$0.00 \rightarrow 0.41e^{-03}\,[s]$
	Δt_h	PMX Sampling Time	$0.41 \rightarrow 1.50e^{-03}\,[s]$
TCF055s	t_s^0	STR DNS Starts	$t = 1.50e^{-03}\,[s]$
	Δt_s^{tran}	STR Settling Time	$1.50 \rightarrow 3.00e^{-03}\,[s]$
	Δt_s	STR Sampling Time	$3.00 \rightarrow 4.00e^{-03}\,[s]$

sage Passing Interface (MPI) for interprocess communication in parallel execution. The algorithm implemented in S3D solves the Navier-Stokes equations for a compressible fluid in conservative form on a structured, Cartesian mesh in one, two or three spatial directions. Spatial derivatives are computed with an eighth-order, explicit, centred, finite-difference scheme (third-order one-sided stencils are used at the domain boundaries in the non-homogeneous directions) in conjunction with a tenth-order, explicit, spatial filter, as described in Ref. [53], to remove high frequency noise and reduce aliasing error. A fourth-order, six-stage, explicit Runge-Kutta scheme, described in Ref. [54], is used for time integration.

The reactive production DNS presented here (premixed and stratified cases including the investigation of hysteresis) were run on 72000 processor cores (for a total computational cost exceeding 50 M CPUhrs) on the TITAN architecture that is part the National Center for Computational Science at Oak Ridge NL (ORNL).

III. RESULTS

In this section DNS of confined turbulent reactive flows are presented, involving flashback in the canonical channel flow configuration. First, plots of instantaneous and averaged quantities are presented to illustrate the different macroscopic behaviour of upstream propagation in the premixed and equivalence ratio-stratified turbulent channel flow configurations (TCF055h and TCF055s). Then, the local flame structure is illustrated and discussed in detail for the premixed and for the stratified flame. Finally, an analysis of the combustion regimes, as suggested from canonical modelling considerations and observed from the DNS datasets of the two flames, is presented.

A. Upstream Flame Propagation

Turbulent flame propagation, against the channel bulk flow, for the premixed and stratified combustion cases is illustrated and discussed below. The unsteady spatial characteristics of the flashback process lack spatial statistical stationarity and, therefore, the plots presented in Sec. III A 2 are built by spatial averaging of the quantities of interest in the homogeneous spanwise direction at arbitrarily chosen time instants. Comparison of these plots with analogous plots from other times (not shown) confirms the absence of any qualitative and quantitative differences between snapshots of the solution during steady propagation in the time intervals Δt_h and Δt_s for premixed and stratified combustion, respectively.

1. Instantaneous Fields

Figure 3 illustrates the flame transitioning between premixed and stratified combustion and the drastic effect of the imposed lean-rich-lean fuel distribution across the channel on the global flame shape. Note that the upper wall is not shown and that the surfaces shown in the plots represent:

- The streamwise velocity normalized by the friction velocity, $u^+ = u/u_\tau$, on the $y^+ = 5$ plane (greyscale contours).
- Hot fluid temperature at $T = 1700\,[K]$ (red iso-surfaces).
- Back-flow regions characterized by negative streamwise velocity located upstream of the flame surface portions that are convex towards the reactants (blue iso-surfaces of $u^+ = 0$).
- The fuel-air equivalence ratio, ϕ, on the $z^+ = 0$ plane (green-to-white "elevation colourscale" contours).

Firstly, it is clear from the sequence of images in Fig. 3 that the spatial variation in local reactivity across the channel, introduced by stratification of the flammable mixture, causes an abrupt, drastic change in flame shape and propagation topology. The flame reactive surface "flips over", during the transient Δt_s^{tran}, and transitions from a propagating mode characterized by the flame front leading-edges located very close to the wall to a radically different propagating mode characterized by a flame front at the channel centreline (V-shaped versus U-shaped propagation). The transition is initiated when

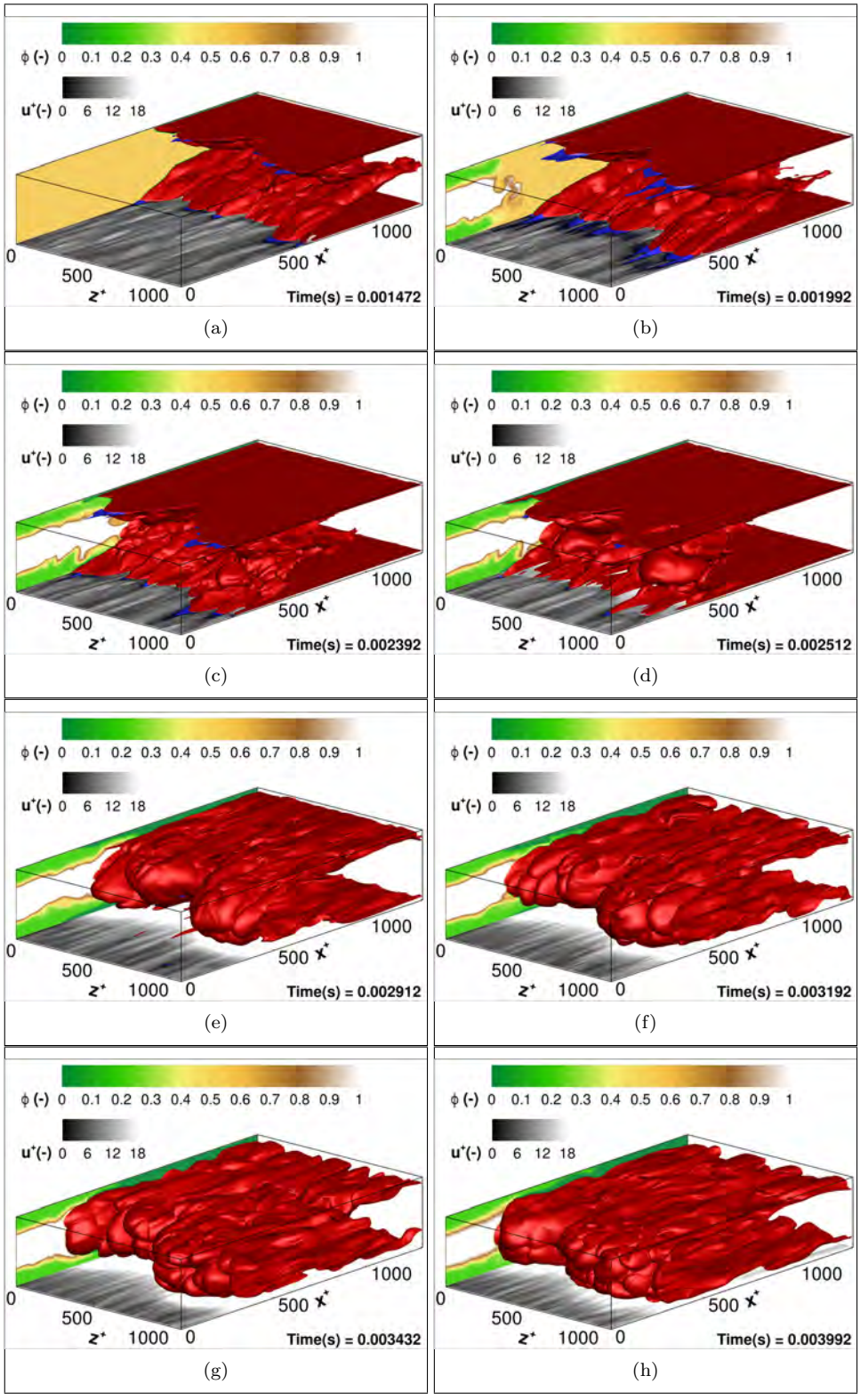

FIG. 3. The transition between premixed combustion and stratified combustion: red iso-surfaces demarcate hot fluid temperature at $T = 1700\,[K]$ while blue iso-surfaces highlight the back-flow regions, $u^+ = 0$. The non-dimensional streamwise velocity (greyscale contours) is shown on the $y^+ = 5$ plane while the equivalence ratio ϕ of the unburnt mixture is illustrated on the $z^+ = 0$ plane (elevation colourscale contours).

the fuel-rich "layer" of the stratified reactants' mixture, convected downstream by the bulk flow, reaches the two upstream-propagating branches of the V-shaped flame. At that point several relatively large "bumps" form on the reactive flame surface approximately 100 wall units from the walls (at $y^+ \sim 100$ and $y^+ \sim 260$) and protrude outwards and upstream into the reactants, see Figs. 3(c) and 3(d), ultimately becoming the flame front leading-edge in the bulk of the channel flow, see Figs. 3(e)-3(h).

Secondly, the change in flame shape induces a subsequent modification of the velocity field in the approaching flow and this has numerous implications on the combustion regime, flame propagation mechanism and possibly hysteresis effects in the flame-flow interaction. In the premixed combustion case, the fresh reactants' flow is deflected away from the walls by the two flame fronts that propagate upstream along the walls as relatively thin flame sheets (V-shaped propagation). It is reasonable to assume that most of the fluid expansion caused by these thin reactive sheets happens in the wall-normal direction [22], a process that ultimately leads to the deflection of the near-wall streamlines away from the walls towards the channel centreline and to the acceleration of the bulk flow of the fresh reactants well upstream of the flame, see also Fig. 5(a) below. Furthermore, the mostly flat near-wall branches of the red isosurfaces in Figs. 3(a)-3(d) evidence a laminarization of the flow in the hot products that closely approach the solid surface in a spatially uniform pattern. Conversely, in the stratified combustion case, the fresh reactants' flow is deflected towards the walls by the reactive front leading-edge. This flame front is now propagating upstream in the fuel-rich bulk flow as a wrinkled turbulent flame sheet of relatively flat mean shape (U-shaped propagation). An acceleration of the fresh reactants' fluid upstream of the flame takes place, in this case, near the walls as clearly evidenced by the grey-to-white transition of u^+ contours at $y^+ = 5$ in the instantaneous plots of Figs. 3(f)-3(h). This time, as opposed to the premixed case, the fluid acceleration along the walls maintains a relatively high turbulence level in the near-wall regions, as evidenced by the strongly wrinkled red isosurfaces in Figs. 3(e)-3(h), and the hot fluid in the products stream approaches the solid surface in the characteristic pattern dictated by the streaky structures of the boundary layer [30].

An additional important observation that can be made on the basis of the instantaneous plots of Fig. 3 concerns the absence, for the U-shaped propagation mode of the stratified flame, of the reverse flow pockets that have been shown to play a central role in premixed flame flashback [21]. This result highlights the existence of a fundamental difference in the physical mechanism of upstream flame propagation for the two configurations considered here. In the premixed case, the presence of low velocity streaks in the near-wall region of the boundary layer allows the appearance of flow reversals that ultimately enable upstream propagation of the flame front causing flashback while, in the stratified case, upstream propagation of the flame front takes place in the bulk flow and its mechanism is therefore unrelated to the streaky structures of the turbulent boundary layer.

Finally, before concluding the present section about the instantaneous fields, it is interesting to mention the considerable difference observed in the wall heat flux instantaneous spatial pattern between the premixed and the stratified case. Fig. 4 illustrates the instantaneous wall heat flux on the lower wall during flashback for the premixed flame 4(a) and for the stratified flame 4(b). While, in the former case, the wall heat flux highest instantaneous values of nearly $2MW/m^2$ are co-located with the entire length and shape of the flame front, in the latter case the highest values of the heat flux are spatially distributed in a quenching pattern, dictated by the interaction of the flame with the boundary layer streaks, that closely resembles the situation described in [30]. This observation suggests that the premixed flame quenches directly at the wall along its leading-edge and, due to the low turbulence level in the hot products downstream of the flame, relatively high values of the wall heat flux are present also in the post-flame region.

2. Averaged Fields

Figure 5 illustrates the spanwise-averaged mean streamwise velocity field, normalized by nominal values of laminar flame speed at $\phi = 0.55$ and $\phi = 1.2$, respectively, and the turbulent fluctuations u'_{rms} normalized by the channel bulk flow velocity, U_{blk}. The most notable observations from the spataially averaged plots can be summarized as follows:

1. In the premixed case, the boundary layers in the fresh reactants upstream of the flame surface thickens due to deflection of the streamlines away from the wall and becomes thinner only in the products stream well past the turbulent flame brush.

2. In the premixed case, the flame front leading edges propagate upstream at a local fluid velocity close to zero (locally in reverse flows).

3. In the premixed case, the bulk flow "feels" the presence of the flame well upstream of its near-wall leading edges and fluid acceleration is already noticeable more than 300 wall units upstream of the flame fronts. Interestingly, this distance is approximately equal to the flame "depth" defined as the spatial length between the flame front leading edges and the the centreline cusp where the two flame branches meet.

4. In the premixed case, relatively weak velocity fluctuations are present throughout the channel attaining a peak value of 1/5 of the bulk flow velocity, U_{blk}, at and immediately downstream of the flame front near-wall leading edges.

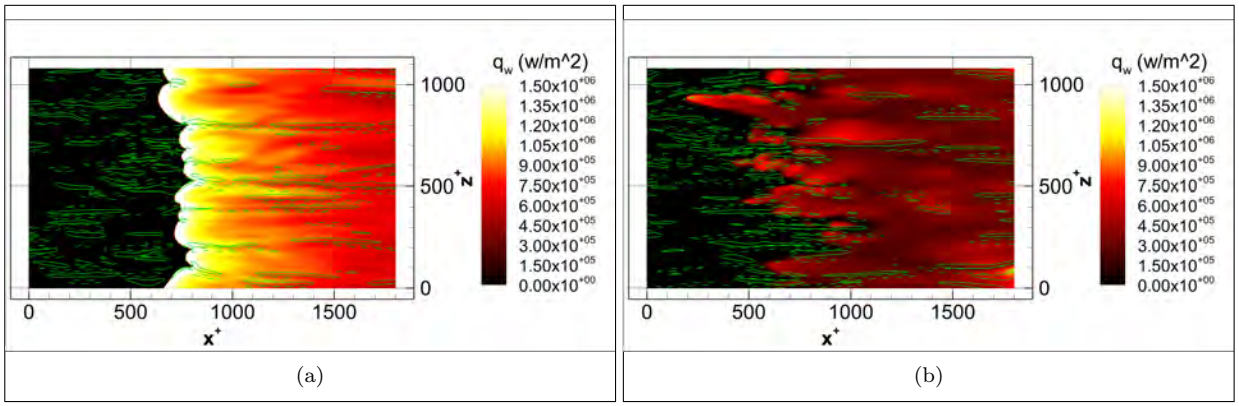

FIG. 4. Instantaneous wall heat flux on the lower wall ($y^+ = 0$) for the premixed 4(a) and stratified case 4(b). The streamwise streaky structures of the boundary layer are demarcated by wall-normal vorticity at $y^+ = 3$ (green lines, solid and dashed lines represent opposite sign of vorticity).

5. In the stratified case, the boundary layers in the fresh reactants "feel" the presence of the flame and become thinner due to deflection of the streamlines towards the walls approximately 200 wall units upstream of the flame front.

6. In the stratified case, the flame front leading edge propagates upstream in the bulk flow against an underlying fluid velocity that equals, on average, twice the corresponding laminar flame speed of the fuel/rich mixture.

7. In the stratified case, strong velocity fluctuations are present at and immediately downstream of the flame front and approximately equal to 1/3 to 1/2 of the bulk flow velocity, U_{blk}.

Based in the aforementioned summary, inspection of the averaged fields confirms and quantifies many of the qualitative observations of Sec. III A 1. The spatially averaged velocity fields, both in the mean and fluctuating parts, inherent to the two flame configurations differ considerably. There exist different physical mechanism that are responsible for the occurrence of flashback in the premixed and in the stratified cases. The spatially averaged temperature fields, shown in Fig. 6, are consistent with the mean velocity fields presented here and with the considerable differences in the instantaneous values of the wall heat fluxes observed in Fig. 4. The thickness of the flame brush, in the mean, is visualized by highlighting (in red) its spatial extent between $C = 0.3$ and $C = 0.7$ for premixed and stratified combustion in Figs. 6(c) and 6(c), respectively. The stratified case exhibits, in the near-wall regions of the flow, a mean flame brush thickness that is considerably larger than that observed in the premixed case (150 versus 50 wall units approximately). An increase in the mean flame thickness can be due to two concurrent physical processes. First, the increased unsteadiness and wrinkling of the instantaneous stratified flame brush can result in an increase of the averaged flame zone thickness. Second, the turbulent length and time scales that characterize the motion of the eddies in the approaching turbulence decrease as the distance from the wall is reduced, due to deflection and acceleration of the mean flow towards the near-wall regions, while the chemical time scales become larger due to locally fuel-lean conditions and heat loss to the wall. The simultaneous occurrence of these processes ultimately causes a considerable change in the local balance between turbulent and chemical time scales (Damköhler/Karlovitz numbers) that, in turn, leads to the entrainment of small eddies in the flame reaction zone. This suggests that the flame may undergo a regime change from thin flamelets near the channel centreline to thickened wrinkled flames closer to the wall. This aspect will be discussed more in detail in Sections III B and III C.

Interestingly, an important common feature characterizes both the premixed and the stratified flame that are, for all other aspects, very different: the slope of the spatially averaged flame surface, represented in Figs. 5 and 6 by the reaction progress variable $C = 0.5$, in the immediate vicinity of the walls. Even if the mean flame surface in the stratified case exhibits a shape that is, for the bulk part, convex towards the reactants' side, very close to the wall, for $y^+ < 10$, the dashed line demarcating the mean flame surface clearly inverts its slope, corresponding to values of the mean streamwise velocity lower than approximately $u_{ave}/S_L = 2$, and approaches the solid, no-slip walls with a slope that is very similar to the one featured in the premixed flame case. This observation suggests the occurrence, within the viscous layer, of similar local balances between flame reactivity, heat loss to the wall and local fluid velocities independent of the actual physical mechanism causing flashback in the channel.

Before concluding the present section about the mean characteristics of the premixed and stratified flames, it

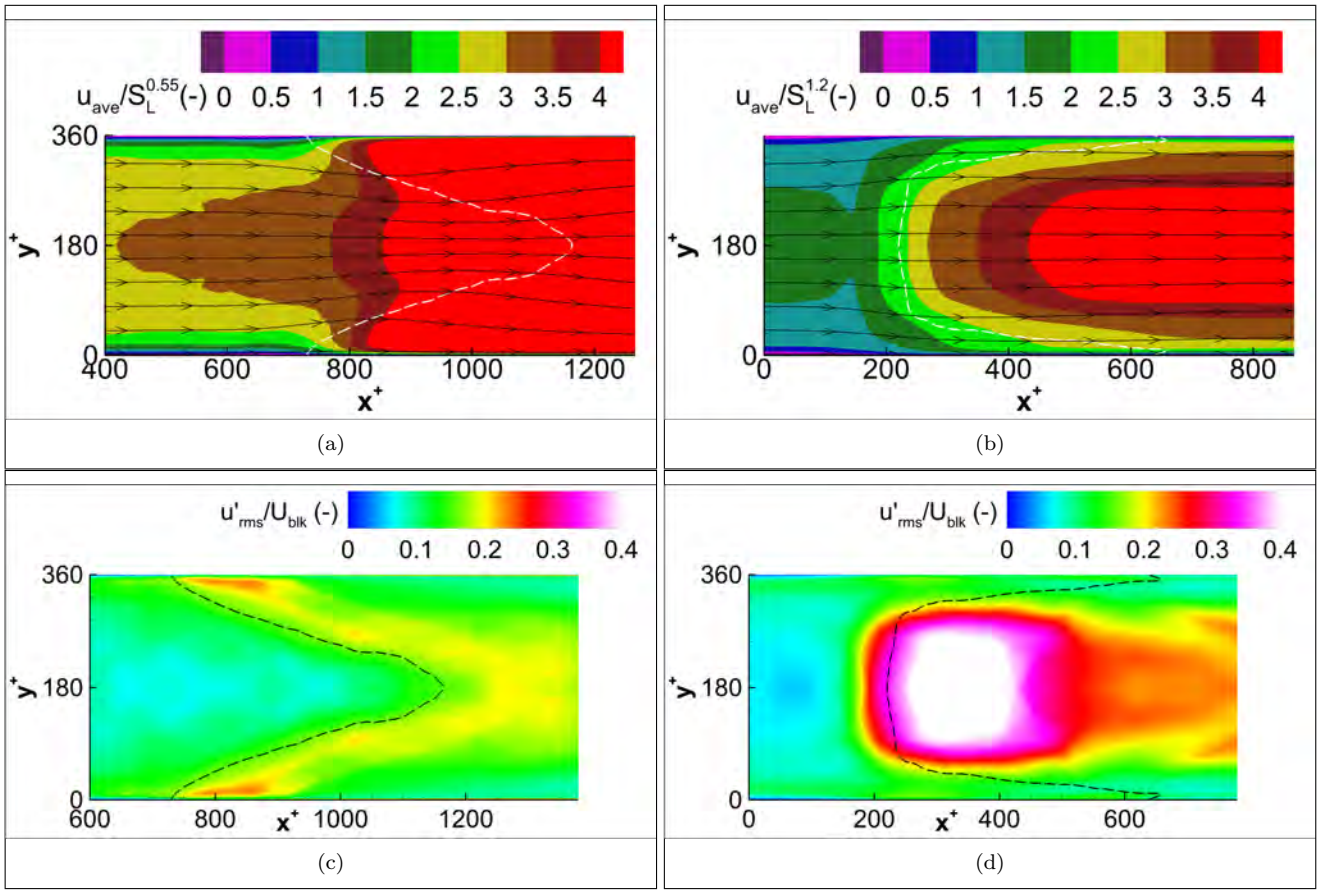

FIG. 5. Mean and fluctuating velocity fields, averaged in the spanwise direction and normalized by the nominal laminar flame speeds (at fuel-rich conditions in the stratified flame case) and by the bulk velocity, U_{blk}, respectively. The flames are denoted by thick dashed lines corresponding to reaction progress variable, $C = 0.5$, and the streamlines by thin black lines with arrowheads for the premixed flame configuration (a)-(c) and for the stratified flame configuration (b)-(d).

is also interesting to consider the eventual occurrence of hysteresis effects in the flow-flame interaction. To this end, the original homogeneous mixture composition is re-introduced at the domain inlet boundary at $x = 0$ once the end of the sampling time Δt_s ($t = 4.00e{-}03[s]$) for the stratified case is reached. The transient that follows (not shown) reveals the occurrence of a reversal of the sequence illustrated in Figs. 3. Notably, the flame transitions back from the U-shaped to the V-shaped propagation mode. This finding suggests that the flow-flame interaction, for the present configurations and compositional changes, is unaffected by hysteresis and that the local reactivity of the reactants mixture approaching the flame is the main governing parameter controlling the mean flame shape, its propagation mechanism and, consequently, the observed flashback characteristics.

B. Local Flame Structure

The local thickness and displacement speed of the flame front are expected to depend on the local equivalence ratio, as well as strain and curvature caused by interaction with the turbulent flow. The interaction of turbulence and flame structure is assessed by evaluating the local progress variable gradient within the flame front. The cross-channel variation of the conditional average progress variable gradient, $\langle \nabla C \mid C = 0.5 \rangle$, conditioned on $C = 0.5$, is shown in Fig. 7(a) for the premixed and equivalence ratio-stratified cases. The figure suggests that the premixed and stratified flames, in spite of the considerable differences in mean shape and approach flow field discussed in the previous section, are characterized by very similar flame thickness in the bulk flow ($60 < y^+ < 300$). The flame thickness of the equivalence ratio-stratified flame increases (∇C reduces) towards the walls. The variation of progress variable gradient within the flame front is shown by presenting the conditional average $\langle \nabla C \mid C \rangle$ versus the progress variable in Fig. 7(b) for the premixed and stratified cases for a range of distances normal to the wall ($y^+ = 3.5, 18, 35, 71, 176$). The thickness of the premixed flame reduces slightly at $y^+ = 3.5$, possibly due to effects of wall heat transfer and reduced tangential strain, however the shape of the

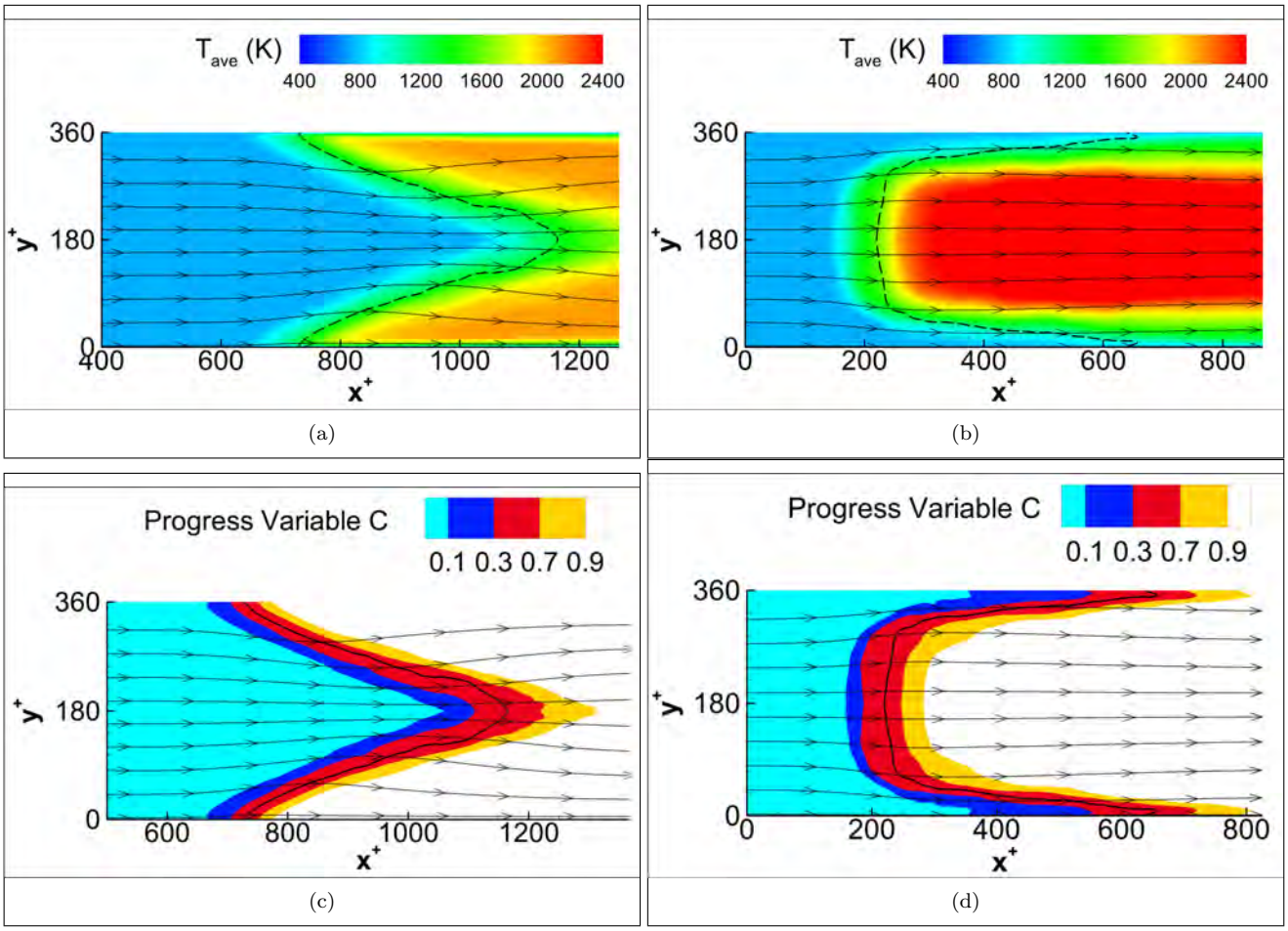

FIG. 6. Mean temperature and reaction progress variable fields, averaged in the spanwise direction, for the premixed flame configuration (a)(c) and for the stratified flame configuration (b)(d). The flame reaction zone is denoted by the black lines corresponding to reaction progress variable, $C = 0.5$.

gradient profile is similar at all wall-normal positions in the premixed flame. For the stratified flame, the shape of the progress variable gradient profile varies significantly from the centre of the channel towards the wall, with progressive flattening of the low-progress variable pre-heat region approaching the wall. The migration of the peak gradient from lower to higher progress variables is partly associated with the variation of equivalence ratio, but thickening of the preheat layer may also be indicative of a change in combustion regime.

A representative value for the turbulent velocity fluctuations u' ahead of the flames is obtained by evaluating the conditional root mean square velocity fluctuation $\langle u'^2 \mid C = 0.05\rangle^{1/2}$ within the pre-heat layer at $C = 0.05$. The u' profiles differ between the premixed and stratified flames; in particular, the stratified case displays a peak in turbulent fluctuations at $y^+ < 5$ (see Sec. III C for more details on this specific topic). However, the increase in flame thickness of the stratified flame near the walls is more closely associated with the variation of equivalence ratio shown in Fig. 7(a). The effect of the equivalence ratio variation on flame behaviour is illustrated in Fig. 7(c) by presenting the mean variation of equivalence ratio across the channel and its effect on the progress variable gradient (at $C = 0.5$) and the propagation speed of freely-propagating planar laminar premixed flames. The laminar flame thickness of hydrogen-air flames determined from H_2O-based progress variable gradients is relatively insensitive to the wide variation of equivalence ratio that characterize the stratified channel flow until the equivalence ratio decreases below 0.25 very close to the walls. In contrast, the equivalence ratio has a marked influence on the laminar flame speed in the region where the local flame thickness is seen to increase in the equivalence ratio-stratified turbulent flame. Therefore the variation of flame thickness in the equivalence ratio-stratified case is largely controlled by an increasing influence of turbulence within the flame, associated with the variation of u'/s_L, rather than by the direct effect of equivalence ratio on local flame front thickness.

The probability density function (PDF) of local flame curvature and tangential strain rate are shown in

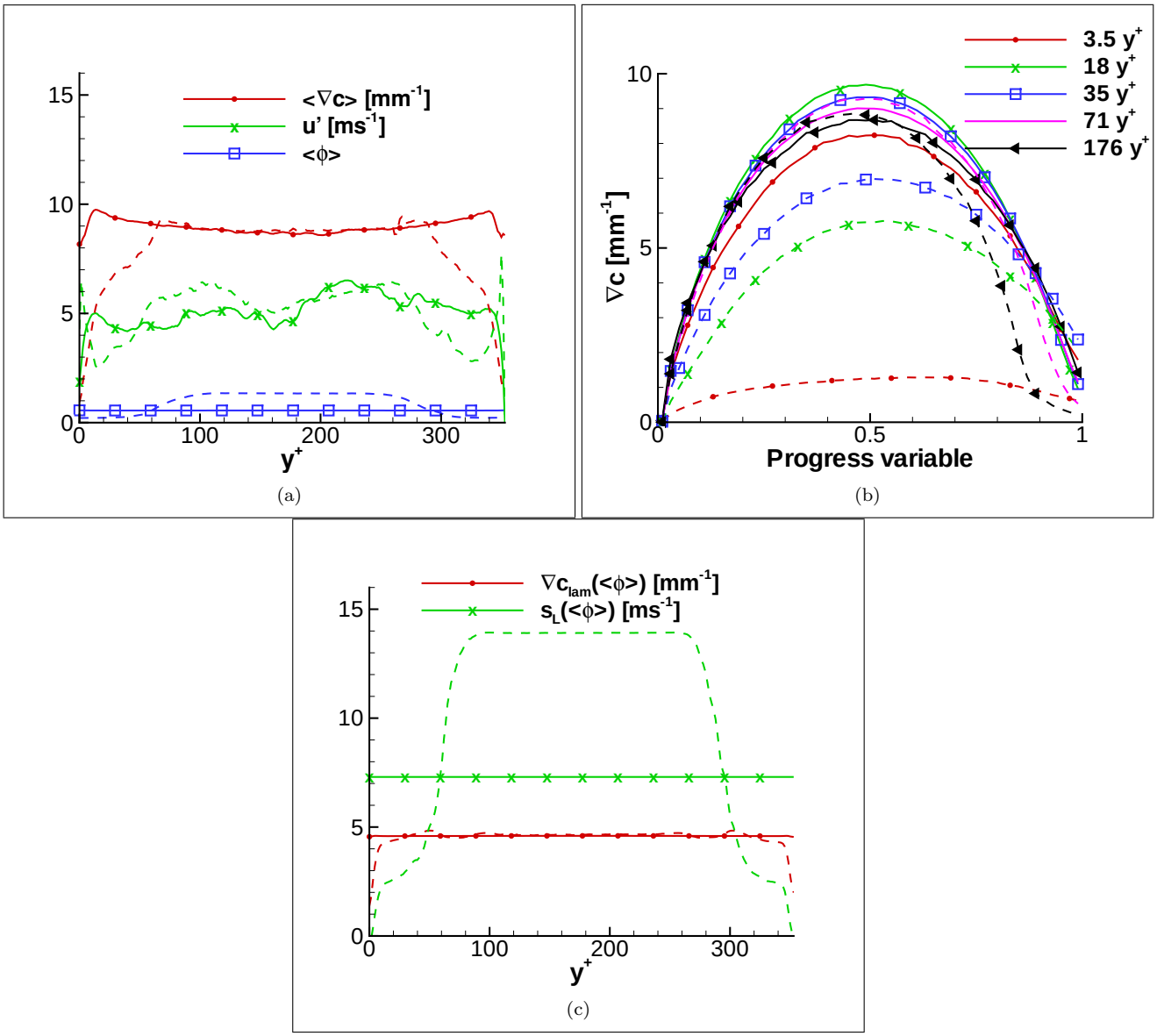

FIG. 7. Variation of the progress variable gradient for the premixed (solid) and equivalence ratio-stratified (dashed) cases: (a) The conditional average progress variable gradient $\langle \nabla C \mid C = 0.5 \rangle$, conditional rms velocity fluctuation $\langle u'^2 \mid C = 0.05 \rangle^{1/2}$, and mean equivalence ratio $\langle \phi \rangle$ across the channel; (b) the variation of the conditional average progress variable gradient through the flame for several y^+ values; (c) laminar flame values of progress variable gradient ∇C_{lam} and flame speed s_L as a function of the mean equivalence ratio at the flame location across the channel.

Figs. 8(a) and 8(b) for a flame surface defined by $C = 0.5$. Positive curvature corresponds to "bulges" convex towards the reactants and negative curvature corresponds to "cusps" concave towards the reactants. The curvature distribution in the premixed flame shows a prevalence of large negative curvature around the centreline $y^+ \sim 176$, corresponding to cusps at the apex of the V-shaped flame. In contrast, the curvature distribution in the stratified flame is approximately symmetric in the centre of the channel. The curvature distribution in the stratified flame has a large positive mean at $y^+ = 3.5$, indicating the prevalence of convex flame bulges as the flame decelerates towards the wall. At intermediate positions, $y^+ = 71$, both the premixed and stratified flames are characterised by mean curvature close to zero with a negatively-skewed distribution, corresponding to bulges of flame meeting at sharp cusps.

Figure8(b) indicates that both flames are characterised by positive mean (extensive) tangential strain, and by positive skewness towards rare high-extensive strain events. The most significant difference between the premixed and equivalence ratio-stratified flames ap-

pears close to the wall (at $y^+ = 3.5$) where the premixed flame exhibits a significant contribution from negative (compressive) tangential strain, characteristic of dilation-driven flame alignment, while tangential strain in the stratified flame remains almost entirely extensive. This may be attributed to the vastly lower contribution of dilatation in the extremely lean mixture at the wall in the stratified case.

C. Combustion Regimes

An accurate prediction of the combustion regimes that characterize flashback in channels and ducts is of primary importance for CFD modelling (RANS, LES) in engineering applications. Most turbulent combustion models routinely utilized in RANS and LES computations are highly tuned to specific combustion regimes, i.e. multi-regime models are complex and not widely adopted yet. Multi-regime models require metrics that delineate the spatio-temporal boundaries between different modes of combustion. Combustion regimes can be described quantitatively by the non-dimensional Damköhler and Karlovitz numbers, both representing the ratio between chemical and turbulent time or length scales that characterize the specific reactive flow, and where energy-containing and dissipative turbulent scales are used respectively [55].

In turbulent channel flows the viscous (wall) time and length scales, t_w and δ_ν, represent well-defined quantities that uniquely characterize the flow. Therefore, in [30] we proposed to utilize the wall time scale t_w, and specifically its value in the undisturbed fresh reactants' flow, to provide a simple, unique ratio to the nominal flame time scale t_l: the wall-based Damköhler number $Da^w = t_w/t_l$, see Tab. II in Sec. II that characterizes the combustion regime in turbulent reactive channel flows. However, in situations where the turbulent and chemical scales span a wide range of values within the same flow, the single valued estimate provided by Da^w may not, in general, be able to accurately delineate variations in combustion regimes. The present DNS datasets correspond to reactive flow configurations that exhibit spatial variations in the turbulent and chemical time scales simultaneously (due to stratification and heat loss), and hence, can be used to assess the accuracy of Da^w to predict the combustion regime(s) occurring across the entire channel width. Furthermore, for those configurations in which Da^w is inaccurate in delineating the different regimes, we propose to construct a *nominal* channel-flow Karlovitz number Ka^{ch}_{in} that provides improved local estimates of the combustion regime as a function of the wall distance. Ka^{ch}_{in} is constructed by utilizing wall-normal profiles of the *nominal* dissipative time scale $t_\eta = (\nu/\epsilon)^{1/2}$ from non-reacting, fully developed channel flows and of the *nominal* chemical time scale $t_l = \delta_l/S_l$ from a table of unstretched laminar premixed flames with consistent stoichiometry, see Fig. 9(a) with the actual mixture conditions from the stratified case. Ka^{ch}_{in} is therefore a *nominal* quantity that can be constructed from tabulated data from turbulent non-reactive channel flows and premixed laminar flames.

Figures 9(b) and 9(c) illustrate a comparison of the *nominal* channel-flow Karlovitz number, Ka^{ch}_{in}, (green lines) against the *effective* Karlovitz number, Ka^{ch}_{fl}, observed in the immediate vicinity of the flame reaction zone (black symbols), where the latter is constructed by sampling local values of t_η and t_l conditional on the reaction progress variable, C, between the 0.1 and 0.3 bounds, *i.e.* these enclose the blue coloured region in Figs. 6(c) and 6(d). In the premixed flame case there is relatively good agreement between the effective channel-flow Karlovitz number and the nominal one which slightly underpredicts the ratio of chemical to turbulent time scales observed at the flame surface. Both combustion regime estimates, the nominal and the effective one, are less than $Ka = 1$, spanning a range of values between 0.4 and 0.9 across the channel. This suggests that the premixed flame is in the "thin flamelets" combustion regime. Note that the single-valued estimate from the wall Damköhler number Da^w is relatively similar to the other two although slightly above unity ($1/Da^w = 1/0.69 = 1.45$). In the stratified flame case Ka^{ch}_{in} underpredicts Ka^{ch}_{fl} in the bulk flow and overpredicts it in the intermediate regions while agreement is quite good near the wall. Clearly both the nominal and the effective Karlovitz number suggest the co-existence of two combustion regimes in the stratified flame configuration: "thin flamelets" in the bulk flow for $Ka < 1$ and "thickened flamelets" in the near-wall regions for $1 < Ka < 10$. It is interesting to note that the present observation of a transition from "thin flamelets" in the bulk flow to "thickened flamelets" near the walls is in good accordance with earlier results from the anchored V-flame configuration [30], characterized by similar mean flame shape (flame leading edge at the channel centreline), and with more recent findings from a DNS study of a turbulent head-on quenching configuration [56], characterized by similar mean direction of the flame-wall interaction (flame brush quenches perpendicularly to the wall).

D. Implications for Flashback Modelling

Although turbulent combustion models validation goes beyond the scope of the present paper, the observations reported in the above Sections provide important guidelines for the choice, development and assessment of such models' ability to represent flame flashback and we summarize these here. This is especially important, and can be of great value, for more applied modeling in connection with coarse-grained RANS and LES approaches characterized by lower computational requirements. First of all, the results presented in Section III A clearly establish that, while accurate prediction of the premixed flame near-wall propagation requires DNS-

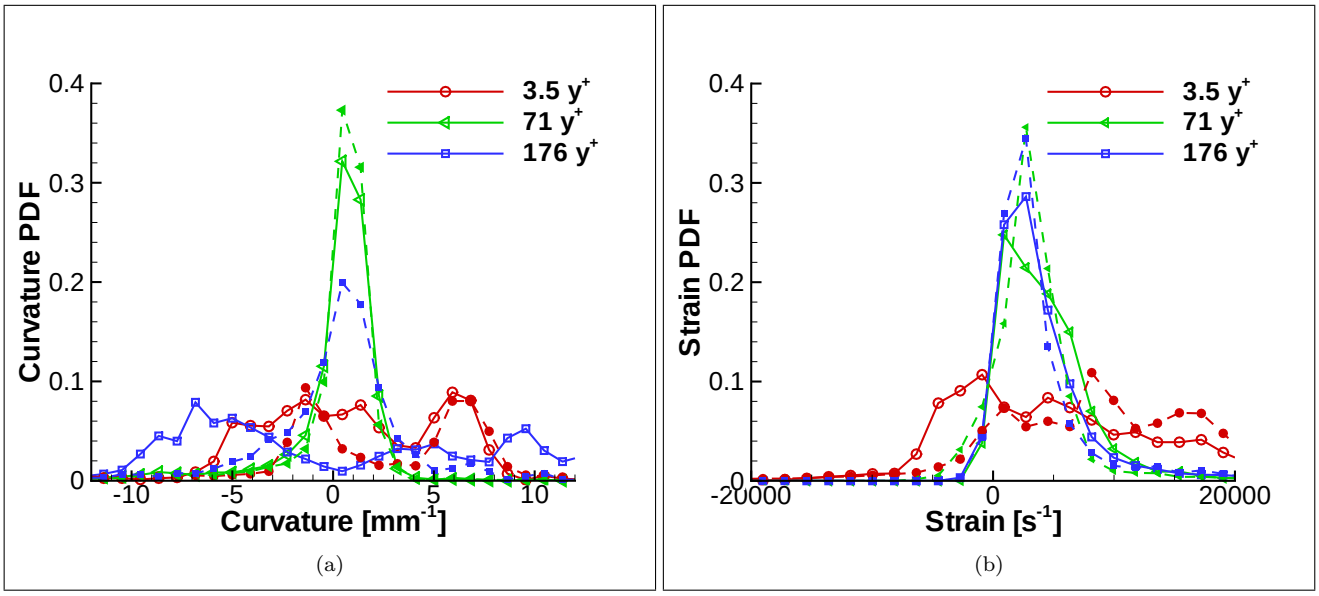

FIG. 8. Probability distributions of (a) curvature and (b) tangential strain rate for the $C = 0.5$ iso-surface at selected wall-normal locations ($y^+ = 3.5, 71, 176$) for the premixed case (solid) and equivalence ratio-stratified case (dashed).

like resolution of the characteristic structures of the wall boundary layer, the stratified flame propagation in the bulk flow is governed by the local turbulent flame velocity and modulated by a relatively homogeneous and more isotropic turbulence present near the channel centreline. Secondly, the discussion from Section III C provides a promising methodology that can be used to estimate the combustion regime of the stratified flame's leading edge that effectively controls propagation of that flame type to the first order. Accordingly, for the present case of relatively low Karlovitz numbers, turbulent combustion models based on a deterministic simplification of the flame surface representation (e.g. flamelet, thickened flame, flame surface density) seem all well-suited to accurately reproduce the stratified flame flashback because they are likely able to accurately capture its governing process: turbulent flame propagation in the bulk flow. As for the premixed flame flashback, general-purpouse turbulent combustion models as those mentioned above are not well-suited to accurately capture the main aspects of this process because it is controlled by unresolved (by the coarse models) details of the near-wall dynamics of the turbulent boundary layer. As promising alternatives, less general and more empirical approaches [22, 24] have shown encouraging results but their applicability is, of course, uncertain outside of the envelope of the datasets used to build them.

IV. CONCLUSIONS

We performed three-dimensional DNSs of upstream flame propagation in fully-developed turbulent plane channel flow for premixed and stratified hydrogen/air flames. The present study complements earlier work [21, 22] and reports a comparison of the flames' shape, structure and propagation mechanism in a fuel-lean homogeneous mixture characterized by an equivalence ratio of $\phi = 0.55$ (premixed flame) and in a globally fuel-lean, non-homogeneous mixture whose equivalence ratio varies between $\phi = 0.2$ at the walls and $\phi = 1.2$ in the bulk flow (stratified flame). The pressure and temperature of the H2/air mixtures is kept the same as in earlier cases, at $P = 2bar$ and $T_u = 750\,[K]$, respectively. The aim of the present DNS study is to investigate the effect of fuel-oxidant mixture stratification on the mechanism of flame flashback in turbulent boundary layers and its implications for the co-existence of multiple combustion regimes.

The introduction of a compositional inhomogeneous reactants' mixture with a fuel lean-rich-lean profile across the channel leads to an abrupt change in the physical mechanism of flame propagation and, in turn, ultimately results in an abrupt change in flame shape and in the related flow pattern. In the premixed configuration (homogeneous mixture) the leading edges of the flame front propagate in the near-wall regions of the turbulent boundary layer, exploiting the low-velocity, streaky coherent structures as they creep upstream under the bulk flow. Conversely, in the stratified configuration (non-homogeneous mixture) the leading edges of the flame front propagate in the bulk flow due to the high reactivity of the fuel-rich mixture injected near the channel centreline. While in the former case the approach flow is deflected away from the walls by the near-wall flame front, in the latter the opposite occurs and the flow is deflected and accelerated towards the walls where turbulence pro-

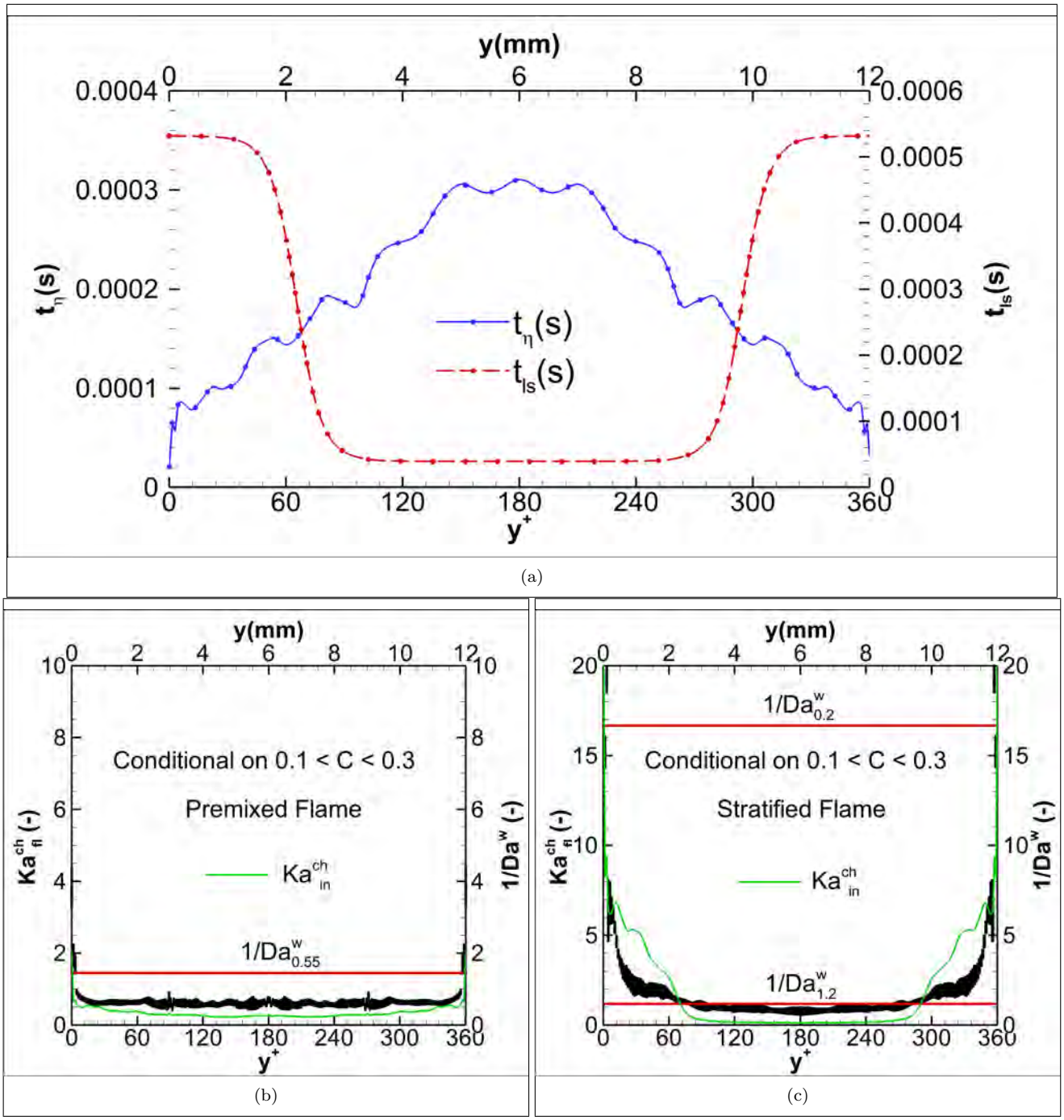

FIG. 9. Wall-normal profiles of turbulent and chemical time scales, t_η (blue line and symbols) and t_{ls} (red line and symbols), are shown at the channel inlet for the stratified combustion case (a). Wall-normal profiles of the *nominal* channel-flow Karlovitz number at the channel inlet plane Ka^{ch}_{in} (green line) and of the *effective* Karlovitz number sampled immediately upstream of the flame Ka^{ch}_{fl} (black symbols, conditionally sampled on $0.1 < C < 0.3$) are shown in the premixed (b) and stratified flame case (c). The reciprocal of the relevant wall Damköhler numbers, Da^w, is also shown (horizontal red lines).

duction occurs. As a consequence the near-wall fuel-lean flame brush encounters relatively strong turbulence ultimately resulting in a combustion regime transition from thin flamelets $Ka < 1$ to thickened flamelets $Ka \sim 10$. Conditionally sampled data (for $C = 0.5$) confirms local thickening of the stratified flame in the near-wall fuel-lean regions of the channel exhibiting lower values of ∇C (versus y^+ and C itself) and the dominance of positive (extensive) strain of the flame surface with the notable exception, in the premixed flame case, of the locations

where reverse flow occurs.

Furthermore, we provide a method to estimate the cross-channel variation of a *nominal* Karlovitz number constructed using canonical time scales for the turbulence and chemistry. Comparison against an *effective* Karlovitz number, computed locally from the DNS data just upstream of the flame reaction layer, reveals a satisfactory agreement between the two. In spite of some level of disagreement observed locally, the present results seem to suggest that the nominal channel-flow Karlovitz, Ka_{in}^{ch}, provides an accurate envelope to its effective counterpart, Ka_{fl}^{ch}. Hence, this implies that an estimate based on Ka_{in}^{ch} can be used to provide an assessment of the combustion regime(s) that characterizes wall-bounded reactive flows in general and can therefore help modellers in selecting the appropriate turbulent combustion modelling approach.

Finally, it is important to recognize that the present analysis has been performed on DNS datasets built at relatively low Reynolds numbers, as it is often the case due to computational cost, and this fact puts some limitations on a broader interpretation of the results. Typically, flashback in gas turbine burners happens at high pressure conditions and this means that a topic of interest is the Reynolds number scaling of the present observations: what is the Reynolds number scaling on the near-wall structures of the turbulent boundary layer that facilitate flashback of the premixed flame along the channel walls? Is the mechanism of upstream flame propagation qualitatively unchanged at higher Reynolds number for the premixed and stratified flames? Given the present limitations of the DNS approach, even in a supercomputing context, laboratory experiments could answer some of these questions. A potentially interesting avenue of investigation that should be pursued experimentally is related to the role on flame flashback of the very large "super structures", recently observed in channel flows at high Reynolds numbers ($Re_\tau > 1000$) using advanced visualization and post-processing techniques [57], that are still beyond the reach of combustion DNS. The presence within the turbulent channel flow of an unsteady meandering "quiescent" core, characterized by high mean longitudinal velocities and low velocity fluctuations level, is likely to have important effects on the mechanisms of upstream flame propagation and result in disruption of the symmetric flame shapes observed here during steady propagation. Intermittently introducing large spatial asymmetries in the channel flow velocity field (see Fig.11 in [57]), these large-scale "super structures" can potentially enhance or hinder flame flashback depending on the relative size of their time scale compared to the flame's own response time scale and to its ability to adapt to changes in the approaching flow field.

V. ACKNOWLEDGEMENT

This publication has been produced with support from the NCCS Centre, performed under the Norwegian research program Centres for Environment-friendly Energy Research (FME). The authors acknowledge the following partners for their contributions: Aker Solutions, ANSALDO Energia, CoorsTek Membrane Sciences, Gassco, KROHNE, Larvik Shipping, Norcem, Norwegian Oil and Gas, Quad Geometrics, Shell, Statoil, TOTAL, and the Research Council of Norway (257579/E20). the work at Sandia National Laboratories was supported by the US Department of Energy, Office of Basic Energy Sciences, Division of Chemical Sciences, Geosciences, and Biosciences. Sandia National Laboratories is a multimission laboratory managed and operated by National Technology and Engineering Solutions of Sandia, LLC., a wholly owned subsidiary of Honeywell International, Inc., for the US Department of Energy's National Nuclear Security Administration under contract DE-NA-0003525. The computational allocation for the present study was provided by the National Infrastructure for High Performance Computing and Data Storage in Norway (project number nn9527k) and by the National Center for Computational Sciences at Oak Ridge National Laboratory, which is supported by the Office of Science of the US Department of Energy under contract DE-AC05-00OR22725.

[1] F. Biagioli, Combustion Theory and Modelling **10**, 389 (2006).
[2] J. Fritz, M. Kröner, and T. Sattelmayer, ASME Journal of Engineering for Gas Turbines and Power **126**, 276 (2004).
[3] A. Kalantari and V. McDonell, Progress in Energy and Combustion Science **61**, 249 (2017).
[4] M. Brower, E. Petersen, W. Metcalfe, H. Curran, M. Füri, G. Bourque, N. Aluri, and F. Güthe, ASME Journal of Engineering for Gas Turbines and Power **135**, 021504 (2013).
[5] N. Donohoe, A. Heufer, W. Metcalfe, H. Curran, M. Davis, O. Mathieu, D. Plichta, A. Morones, E. Petersen, and F. Güthe, Combustion and Flame **161**, 1432 (2014).
[6] A. Sanchez and F. Williams, Progress in Energy and Combustion Science **41**, 1 (2014).
[7] F. Dabireau, B. Cuenot, O. Vermorel, and T. Poinsot, Combustion and Flame **135**, 123 (2003).
[8] P. Chiesa, G. Lozza, and L. Mazzocchi, ASME Journal of Engineering for Gas Turbines and Power **127**, 73 (2005).
[9] D. Ebi and N. Clemens, Combustion and Flame **168**, 39 (2016).
[10] D. Ebi, R. Ranjan, and N. Clemens, Experiments in Fluids **59**, 109 (2018).

[11] A. Masri, in *Proceedings 35th International Symposium on Combustion* (The Combustion Institute, 2015) pp. 1115–1136.

[12] R. Grout, A. Gruber, C. Yoo, and J. Chen, Proceedings of the Combustion Institute **33**, 1629 (2011).

[13] R. W. Grout, A. Gruber, H. Kolla, P.-T. Bremer, J. C. Bennet, A. Gyulassy, and J. H. Chen, Journal of Fluid Mechanics **706**, 351 (2012).

[14] H. Kolla, R. Grout, A. Gruber, and J. Chen, Combustion and Flame **159**, 2755 (2012).

[15] Y. Minamoto, H. Kolla, R. Grout, A. Gruber, and J. Chen, Combustion and Flame **162**, 3569 (2015).

[16] F. Biagioli and F. Güthe, Combustion and Flame **151**, 274 (2007).

[17] B. Lewis and G. von Elbe, Journal of Chemical Physics **11**, 75 (1943).

[18] A. Dreizler and B. Bø"hm, in *Proceedings 35th International Symposium on Combustion* (The Combustion Institute, 2015) pp. 37–64.

[19] C. Eichler and T. Sattelmayer, Experiments in Fluids **52**, 347 (2012).

[20] C. Heeger, R. L. Gordon, , M. J. Tummers, T. Sattelmayer, and A. Dreizler, Experiments in Fluids **49**, 853 (2010).

[21] A. Gruber, J. H. Chen, D. Valiev, and C. K. Law, Journal of Fluid Mechanics **709**, 516 (2012).

[22] A. Gruber, A. R. Kerstein, D. Valiev, C. K. Law, H. Kolla, and J. H. Chen, in *Proceedings 35th International Symposium on Combustion* (The Combustion Institute, 2015) pp. 1485–1492.

[23] G. Baumgartner, L. R. Boeck, and T. Sattelmayer, in *Proceedings of the ASME Turbo Expo 2015, June 15-19 2015, Montreal, Canada* (American Society of Mechanical Engineers, 2015) pp. GT2015–42605.

[24] V. Hoferichter, C. Hirsch, and T. Sattelmayer, Combustion Theory and Modelling **21**, 382 (2017).

[25] B. Fine, Combustion and Flame **2**, 253 (1958).

[26] L. Khitrin, P. Moin, D. Smirnov, and V. Shevchuk, in *Proceedings 10th International Symposium on Combustion* (The Combustion Institute, 1965) pp. 1285–1291.

[27] V. N. Kurdyumov, E. Fernandez, and A. Linan, Proceedings of the Combustion Institute **28**, 1883 (2000).

[28] V. N. Kurdyumov and E. Fernandez-Tarrazo, Combustion and Flame **128**, 382 (2002).

[29] V. N. Kurdyumov, E. Fernandez-Tarrazo, J. M. Truffaut, J. Quinard, A. Wangher, and G. Searby, Proceedings of the Combustion Institute **31**, 1275 (2007).

[30] A. Gruber, R. Sankaran, E. R. Hawkes, and J. H. Chen, Journal of Fluid Mechanics **658**, 5 (2010).

[31] C. Eichler and T. Sattelmayer, ASME Journal of Engineering for Gas Turbines and Power **133**, 011503 (2011).

[32] C. Eichler, G. Baumgartner, and T. Sattelmayer, in *Proceedings of ASME Turbo Expo 2011, June 6-10, 2011, Vancouver, Canada* (American Society of Mechanical Engineers, 2011) pp. GT2011–45362.

[33] A. Gruber, P. S. Salimath, and J. H. Chen, International Journal of Hydrogen Energy **39**, 5906 (2014).

[34] R. J. Kee, G. Dixon-Lewis, J. Warnatz, M. E. Coltrin, J. A. Miller, and H. K. Moffat, *A Fortran Chemical Kinetics Package for the Analysis of Gas-Phase Chemical Kinetics*, Tech. Rep. Release 3.5 (Reaction Design Inc., San Diego, CA, 1999).

[35] J. Li, Z. Zhao, A. Kazarov, and F. L. Dryer, International Journal of Chemical Kinetics **36**, 566 (2004).

[36] T. Poinsot and S. K. Lele, Journal of Computational Physics **101**, 104 (1992).

[37] J. C. Sutherland and C. A. Kennedy, Journal of Computational Physics **191**, 502 (2003).

[38] C. S. Yoo, Y. Wang, A. Trouvé, and H. G. Im, Combustion Theory And Modelling **9**, 617 (2005).

[39] C. S. Yoo and H. G. Im, Combustion Theory And Modelling **11**, 259 (2007).

[40] A. Gruber, *Direct Numerical Simulation Of Turbulent Combustion Near Solid Surfaces*, Doctoral thesis, Norwegian University of Science and Technology (2006).

[41] R. Moser, J. Kim, and N. Mansour, Physics of Fluids **11**, 943 (1999).

[42] J. H. Chen, A. Choudhary, B. de Supinski, M. DeVries, E. R. Hawkes, S. Klasky, W. K. Liao, K. L. Ma, J. Mellor-Crummey, N. Podhorski, R. Sankaran, S. Shende, and C. S. Yoo, Computational Science and Discovery **2**, 1 (2009).

[43] E. R. Hawkes and J. H. Chen, in *Proceedings 30th International Symposium on Combustion* (The Combustion Institute, 2005) pp. 647–655.

[44] R. Sankaran, E. R. Hawkes, J. H. Chen, T. Lu, and C. K. Law, in *Proceedings 31th International Symposium on Combustion* (The Combustion Institute, 2007) pp. 1291–1298.

[45] E. Hawkes, O. Chatakonda, H. Kolla, A. Kerstein, and J. Chen, Combustion and Flame **159**, 2690 (2012).

[46] E. R. Hawkes, R. Sankaran, J. C. Sutherland, and J. H. Chen, in *Proceedings 31th International Symposium on Combustion* (The Combustion Institute, 2007) pp. 1633–1640.

[47] C. S. Yoo, R. Sankaran, and J. H. Chen, Journal of Fluid Mechanics **640**, 453 (2009).

[48] E. Richardson and J. Chen, Proceedings of the Combustion Institute **36**, 1729 (2017).

[49] H. Wang, E. Hawkes, B. Savard, and J. Chen, Combustion and Flame **193**, 229245 (2018).

[50] T. Echekki and J. H. Chen, Combustion and Flame **134**, 169 (2003).

[51] R. Sankaran, H. G. Im, E. R. Hawkes, and J. H. Chen, in *Proceedings 30th International Symposium on Combustion* (The Combustion Institute, 2005) pp. 875–882.

[52] A. Konduri, A. Gruber, C. Xu, T. Lu, A. Krisman, M. Bothien, and J. Chen, Proceedings of the Combustion Institute **In Press**, xxx (2019).

[53] C. A. Kennedy and M. H. Carpenter, Applied Numerical Mathematics **14**, 397 (1994).

[54] C. A. Kennedy, M. H. Carpenter, and R. M. Lewis, Applied Numerical Mathematics **35**, 177 (2000).

[55] R. Borghi, Progress in Energy and Combustion Science **14**, 245 (1988).

[56] P. Zhao, L. Wang, and N. Chakraborty, Journal of Fluid Mechanics **848**, 193 (2018).

[57] Y. Kwon, J. Philip, C. de Silva, N. Hutchins, and J. Monty, Journal of Fluid Mechanics **751**, 228 (2014).